Inorganic Chemistry

Article

pubs.acs.org/IC

Photocatalytic Hydrogen Generation System Using a Nickel-Thiolate Hexameric Cluster

Husain N. Kagalwala,[†] Eric Gottlieb,[†] Gao Li,[†] Tao Li,[‡] Rongchao Jin,[†] and Stefan Bernhard*[,†]

[†]Department of Chemistry, Carnegie Mellon University, 4400 Fifth Avenue, Pittsburgh, Pennsylvania 15213, United States

[‡]Department of Chemistry, University of Pittsburgh, Chevron Science Center, 219 Parkman Avenue, Pittsburgh, Pennsylvania 15260, United States

Supporting Information

ABSTRACT: We report the use of a nickel-thiolate hexameric cluster, $Ni_6(SC_2H_4Ph)_{12}$, for photocatalytic hydrogen production from water. The nickel cluster was synthesized ex-situ and characterized by various techniques. Single crystal X-ray analysis, ^1H NMR, 2D COSY, ESI-MS, UV−visible spectroscopy, and TGA provided insight into the structure and confirmed the purity and stability of the cluster. Cyclic voltammetry helped confirm hydrogen evolution reaction (HER) activity of this catalyst. Photoreactions carried out using an iridium photosensitizer, $Ir(F\text{-}mppy)_2(dtbbpy)[PF_6]$, and TEA as the sacrificial reductant revealed the high activity of the Ni_6 cluster as a water reducing catalyst. High TONs (3750) and TOFs (970 h^{-1}) were obtained at optimum catalyst concentration (0.025 mM), with low concentrations of catalyst yielding up to 30 000 turnovers. Quenching studies, along with the evidence obtained from the electrochemical analysis, showed that this water reduction system proceeds through a reductive quenching mechanism. Mercury poisoning studies confirmed that no active, metallic colloids were formed during the photocatalytic reaction.

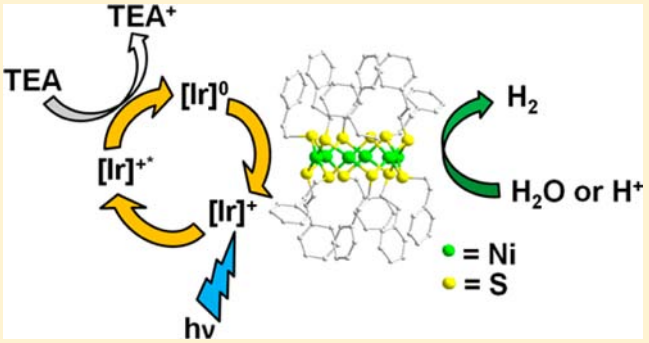

INTRODUCTION

The global increase in CO_2 emissions due to uninhibited fossil fuel use has led to an intense search for alternate fuels that are equally efficient as well as benign to the environment. An exciting alternative would be to use a carbon-neutral energy source like sunlight to generate hydrogen from clean abundant sources.[1] Photolysis of water, a plentiful resource, into hydrogen and oxygen thus serves as a promising avenue to generate both sustainable fuel and oxidant. However, due to the complexity involved in the 4-electron−4-proton transfer process, water splitting is usually addressed as two separate problems: water oxidation and reduction.[2] The basic photocatalytic water reduction system involves three components: a light-absorbing photosensitizer (PS), water-reducing catalyst (WRC), and a sacrificial reductant (SR) which replaces the complex water oxidation half-reaction. While a majority of the work done in this area involves the use of transition-metal-based PSs with noble[3] and non-noble metal containing WRCs,[4] recent works eliminate the use of expensive metals by utilization of organic dyes in combination with nonprecious metal-based catalysts.[5] The latter systems, in spite of showing good activity, suffer from low turnovers, mainly due to the reduction catalyst instability and subsequent photodegradation of the dye.[5a]

In an effort to find stable earth-abundant WRCs, chemists have been exploring different ligand−metal systems; nickel thiolates, in particular, have gained special importance because of their structural similarity to the active site in [Ni−Fe] hydrogenase.[6] An important strategy involves ligand modification and experimenting with the electronic environment surrounding the metal. Hence, several types of nickel thiolates have been synthesized and used for photogeneration of hydrogen.[7] Nickel-thiolate cluster complexes are a class of compounds which drew our attention because of the unique structural possibilities which could be achieved by modification of the corresponding thiolate ligand.[8] More importantly, some of these clusters have also been shown to reduce protons electrocatalytically.[9] There are, however, very few reports on photocatalytic water reduction properties of such clusters. Recently, Zhang et al. demonstrated that an in-situ formed nickel hexameric cluster could be used as a WRC along with Erythrosin B as the PS, with the system exhibiting a quantum efficiency of 24.5% at 460 nm.[10]

In this Article, we investigate photocatalytic water reduction by using an earth-abundant metal (nickel)-containing thiolate cluster with an iridium-based PS. The nickel catalyst used for this purpose was a phenylethylthiolate-based tiara-like cluster, $Ni_6(SC_2H_4Ph)_{12}$ or $Ni_6(PET)_{12}$ which was synthesized ex-situ and characterized by various techniques which shed light on its

Received: May 24, 2013
Published: July 18, 2013

   dx.doi.org/10.1021/ic4013069 | Inorg. Chem. 2013, 52, 9094−9101

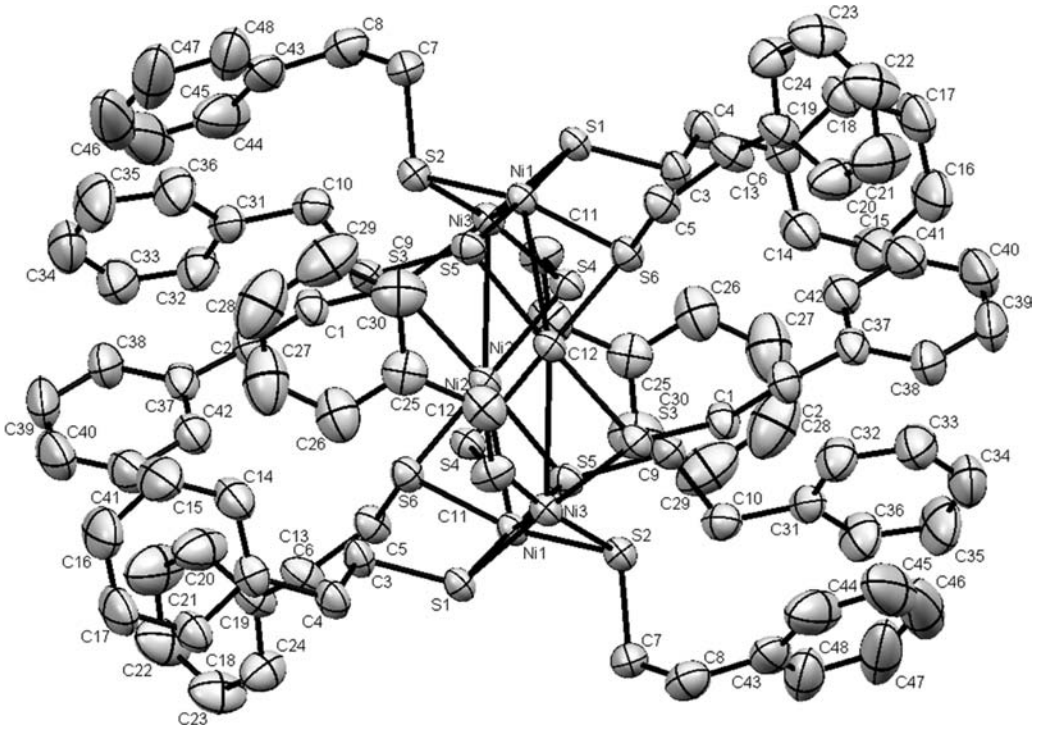

Figure 1. Thermal ellipsoid diagram showing the hexameric double crown-like Ni_6S_{12} core.

structural aspects as well as its purity. Electrochemical analysis demonstrated the proton reducing ability of the Ni cluster, justifying its use as a water reducing catalyst. A cyclometalated Ir(III) complex, $[Ir(F\text{-}mppy)_2(dtbbpy)](PF_6)$, was chosen as the PS since this complex has been shown to be a very robust and versatile $[Ir(C^N)(N^N)]^+$ derivative, exhibiting a high emission lifetime and excited state reduction potential.[3b,11] Careful optimization of the overall system led to high performances in terms of catalytic turnover numbers (TONs) and turnover frequencies (TOFs). Quenching studies further elucidated the catalytic mechanism observed in this water reduction system while mercury poisoning test helped ascertain the absence of reactive metallic colloids.

EXPERIMENTAL SECTION

Chemicals and Materials. Iridium(III) chloride ($IrCl_3{\cdot}H_2O$) was purchased from Pressure Chemicals. 4,4′-di-tert-butyl-2,2′-bipyridine (dtbbpy), nickel(II) chloride ($NiCl_2{\cdot}6H_2O$), 2-phenylethanethiol (PhC_2H_4SH, 99%), sodium borohydride ($NaBH_4$, 99.99%), tetrahydrofuran (THF, HPLC grade), and dichloromethane (CH_2Cl_2, HPLC grade, 99%) were obtained from Sigma-Aldrich. Tetraoctylammonium bromide (TOABr > 98%) and tetra-n-butylammonium hexafluorophosphate (TBAH, 99%) were purchased from Fluka. All chemicals were used without further purification. Nanopure water (18.2 MΩ cm) was used in all experiments that involve water.

Synthesis of F-mppy and $[Ir(F\text{-}mppy)_2(dtbbpy)](PF_6)$. The cyclometallating ligand, 5-methyl-2-(4-fluorophenyl)pyridine (F-mppy), and the iridium complex were synthesized according to procedures reported previously.[11]

Synthesis of $Ni_6(PET)_{12}$. This material was synthesized using modified literature procedures employed previously for Au and Pd-based nanoclusters.[12] All steps were performed under air atmosphere and at room temperature. $NiCl_2{\cdot}6H_2O$ (0.1000 g, 0.42 mmol) and TOABr (0.488 g, 0.89 mmol) were first dissolved in 100 mL of THF to give a deep-blue solution. Phenylethanethiol (0.290 mL, 2.17 mmol) was added, and the reaction mixture was stirred for an additional 5 min. This was followed by addition of $NaBH_4$ (0.160 g, 4.23 mmol) dissolved in 14 mL of cold water, leading to the formation of a dark-brown solution, indicating the formation of the nickel product. The reaction continued to stir for typically 24 h. To isolate the crude product, THF was removed via rotary evaporation at room temperature. A water phase and an oily phase containing the product remained. The oily phase was washed with methanol three times to remove excess phenylethanethiol followed by extraction with CH_2Cl_2 twice, leaving behind an insoluble solid. The isolated crude product was crystallized by dissolving in a minimum amount of CH_2Cl_2, adding an equal volume of ethanol, and setting aside for slow evaporation of CH_2Cl_2. Crystals typically formed within 24 h but were left for up to 1 week. Crystals were separated by washing with ethanol 3 times and drying under vacuum (30−35% yield).

^{1}H NMR (300 MHz, chloroform-*d*): δ 6.8−7.3 (m, 60 H), 3.18 (t, 12 H), 2.62 (t, 12 H), 2.46 (t, 12 H), 1.89 (t,12 H). MS (*m*/*z*, ESI): 2131.09 (100%, $[M + Cs]^+$)

Characterization of $Ni_6(PET)_{12}$. Single crystal X-ray data of $Ni_6(PET)_{12}$ was collected on a Bruker X8 Prospector Ultra equipped with an Apex II CCD detector and an IμS microfocus Cu Kα X-ray source (λ = 1.541 78 nm). The data was collected at room temperature (296 K). ^{1}H NMR and 2D correlation spectra (COSY) were recorded on Bruker 300 MHz spectrometer at room temperature. Positive ion electrospray ionization mass spectrometry (ESI-MS) was performed using a Waters Q-TOF mass spectrometer equipped with Z-spray source. Experimental details are given in the Supporting Information (SI). UV−vis spectra of the products were measured using an HP Agilent 8453 diode array spectrophotometer at room temperature. Thermogravimetric analysis (TGA) was done on a TG/DAT6300 analyzer (Seiko Instruments, Inc.) under a N_2 atmosphere (flow rate ∼50 mL/min).

Electrocatalytic Proton Reduction. Proton reduction experiments were carried out using a CH-Instruments electrochemical analyzer model 600C potentiostat. Increasing equivalents of glacial acetic acid (AcOH) were added to a 0.1 M solution of TBAH in THF containing 1 mM Ni_6 catalyst. A 3 mm glassy carbon working electrode, coiled platinum wire counter electrode, and a silver wire pseudoreference electrode were employed for the measurements. Ferrocene (Sigma) was used as an internal standard, and all potentials were referenced to the standard calomel electrode (SCE).[13]

dx.doi.org/10.1021/ic4013069 | Inorg. Chem. 2013, 52, 9094−9101

Photoreaction Protocol. All solutions were made in 40 mL screw top vials (VWR). Specified amounts of PS and catalyst were dissolved in the solvent (10 mL) which comprised 8 mL of THF, 1 mL of H_2O and 1 mL of TEA. The vials were then placed in a 16 well, water-cooled LED photoreactor which is mounted on an orbital shaker. Pressure transducers were screwed onto the vials before they were subjected to degassing by applying vacuum, which was followed by filling them with Ar gas. This cycle was repeated 7 times before allowing the vial headspace to come to atmospheric pressure. The orbital shaker was turned on (100 rpm), and the samples were illuminated from below using the LEDs (460 nm). H_2 generation was monitored with the help of pressure transducers, and the corresponding kinetic traces were obtained. The reactions were run till no more increase in the H_2 evolution traces was observed. The reaction headspace of each vial was then analyzed using a residual gas analyzer (RGA) which had been previously calibrated using 1:9 and 3:7 H_2–Ar mixtures. Pressure outputs from the samples were referenced against vials containing only the solvent. All reactions were carried out at room temperature.

RESULTS AND DISCUSSION

Ni_6 Cluster Structure Elucidation. Single crystal X-ray analysis established the metallocrown-like structure, containing six Ni atoms arranged in an approximately hexagonal ring, with six bridging sulfur atoms above and six below the plane (Figure 1). The crystal was found to belong to the $P2_1/n$ space group, having a primitive monoclinic unit cell with dimensions a = 11.3690(13) Å, b = 12.5599(17) Å, c = 32.770(3) Å, α = 90.00(0)°, β = 91.729(9)°, and γ = 90.00(0)°. Each Ni ion has a distorted square planar geometry. Details of the crystal structure and atomic parameters are given in the SI.

Further insight into the structural features was gained via ^{1}H NMR (in $CDCl_3$) which displayed four triplets in the aliphatic region as depicted in Figure 2A. The peaks at 3.18 and 2.62 ppm belong to the α-methylene (attached to S) protons, while β-methylene protons give rise to the peaks at 2.46 and 1.89 ppm. The reason for these two sets of peaks is attributed to the alternate axial and equatorial placement of the ligands around the hexameric core, caused by the steric bulk of the ligands. More evidence was obtained from a 2D COSY experiment (Figure 2B) which confirms the existence of two groups of protons, group 1 (3.18 and 2.46 ppm) and group 2 (2.62 and 1.89 ppm), confirming the presence of two different ligand environments. Similar structural arrangements have been seen in PET protected gold nanoclusters[14] as well as other $[M(SR)_2]_6$ complexes (M = Ni, Pd, etc.).[15]

Positive ion ESI-MS analysis shows the presence of a peak at m/z = 2131.09, as depicted in Figure 3. This peak corresponds to the nickel hexameric adduct $[Ni_6(PET)_{12} + Cs]^+$. Of note, to impart charges to the neutral $Ni_6(PET)_{12}$ via cesium-adduct formation the cluster solution was mixed with cesium acetate prior to ESI-MS analysis. The other peaks (with spacing of 192, i.e., the mass of CsOAc) are from $[CsOAc]_nCs^+$ adducts; for example, m/z = 1284.41 is from $[CsOAc]_6Cs^+$. All the experimental isotope peak features match exactly with the simulated pattern, further confirming the $Ni_6(PET)_{12}$ formula (Figure S1, SI).

UV–visible spectroscopic analysis of the Ni_6 cluster showed the presence of three charge transfer bands (Figure S2, SI) which is due to the low spin NiS_4 environment of Ni^{II} ion.[9] The cluster remains stable in solution for several days, with little decrease in intensity of the peaks (Figure S3,SI). In the presence of acetic acid (AcOH) and photoreaction solvent, the cluster degrades slowly over a period of 24 h, with retention of the Ni_6 features (Figure S4, SI). Furthermore, no change in the

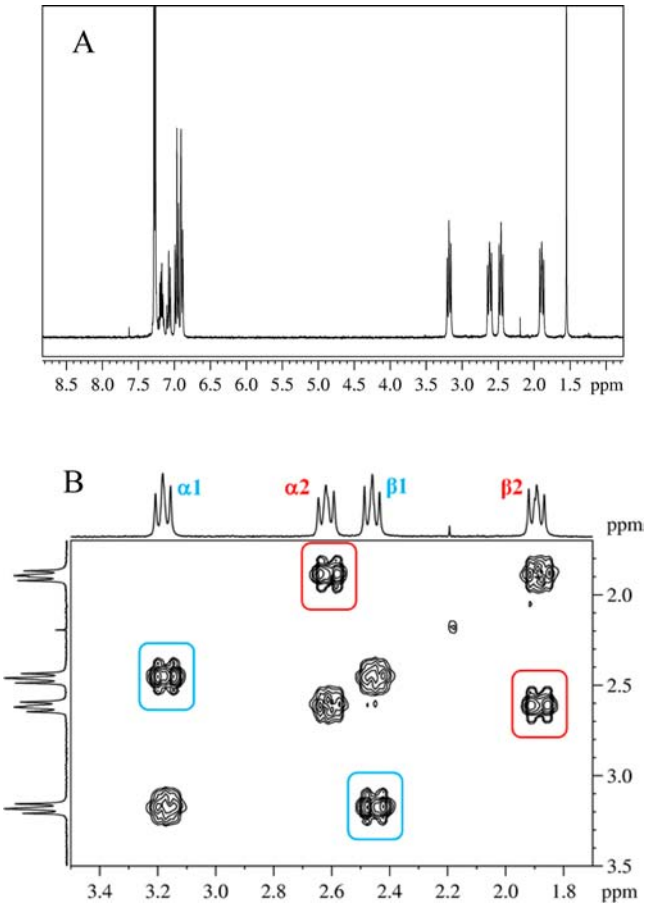

Figure 2. (A) ^{1}H NMR and (B) 2D COSY spectra of $Ni_6(PET)_{12}$ showing the presence of two different ligand orientations due to steric bulk of the thiolate ligands. (RT, $CDCl_3$ solvent).

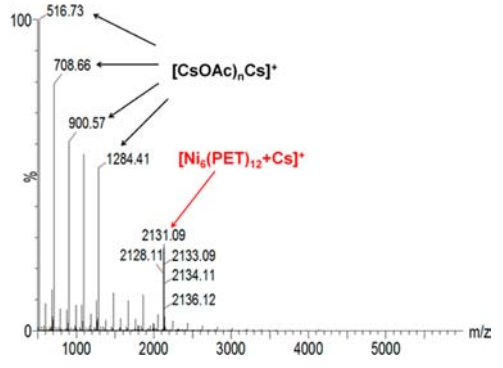

Figure 3. Positive ESI-MS of $Ni_6(PET)_{12}$. The peak at m/z = 2131.09 could be attributed to nickel cluster Cs adduct, $[Ni_6(PET)_{12} + Cs]^+$. The remaining peaks can be assigned to adducts of the type $[CsOAc]_nCs^+$.

^{1}H NMR spectrum was seen on addition of increasing equivalents of AcOH and after 24 h (Figures S5 and S6, SI), outlining the stability of the cluster in acidic environment. TGA shows that the cluster is thermally stable up to 200 °C and undergoes a weight loss of approximately 72%, corresponding to the carbon and hydrogen content of the complex (Figure S7, SI).

$Ni_6(PET)_{12}$ as a Hydrogen Evolution Reaction (HER) Catalyst. To determine the role of the Ni_6 cluster as an HER catalyst, cyclic voltammetry was performed in the presence of

dx.doi.org/10.1021/ic4013069 | Inorg. Chem. 2013, 52, 9094–9101

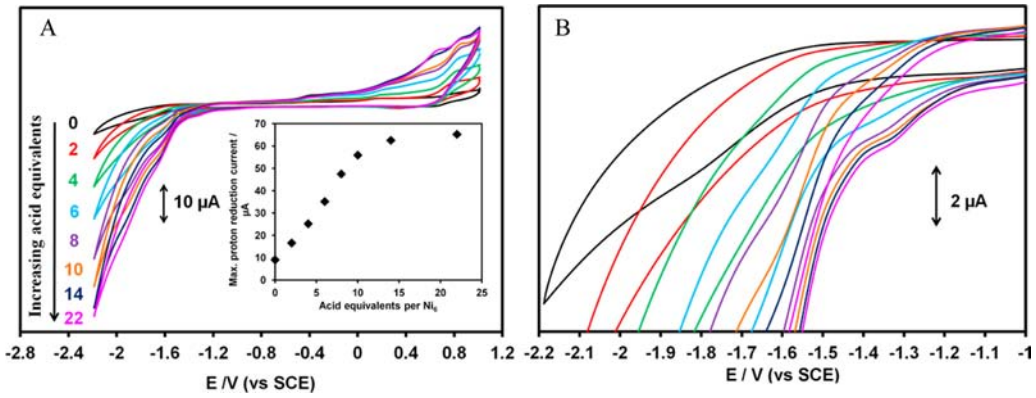

Figure 4. (A) Cyclic voltammograms of $Ni_6(PET)_{12}$ demonstrating proton reduction in presence of acid. Inset: Effect of acid concentration on proton reduction current. (B) Reduction waves of $Ni_6(PET)_{12}$ demonstrating the reduction of the cluster at more positive potentials in presence of increasing acid equivalents. Scan rate = 100 mV/s.

increasing amounts of AcOH. In the absence of acid (Figure 4A, black line), the cluster shows a very weak irreversible reduction wave around −1.8 V (Ni^{II} to Ni^{I}) and an irreversible oxidation (Ni^{II} to Ni^{III}) at +0.8 V. On addition of acid, an increase in current is seen and a more pronounced Ni reduction peak begins to form at a more positive potential of −1.4 V (Figure 4B, blue line, 6 acid equivalents). This peak continues to shift slightly with increasing acid concentration and finally centers at −1.32 V. This observation indicates direct protonation of the reduced Ni(I) center and also that the protonation is faster than the overall catalytic rate.[16] It is important to note that the Ni(II/I) potential also lines up well with the reduction potential of the Ir PS, rendering electron transfer between the species feasible during photocatalysis. Moreover, a new reductive event appears at −1.6 V, the current height of which increases with increasing acid equivalents. This can be attributed to electrochemical desorption, leading to H_2 evolution. Similar observations have been reported by various groups employing Ni-based HER catalysts.[5b,9,17] The H_2 liberation current reaches saturation after adding 22 equiv of acid (Figure 4A, inset).

An electrode rinsing experiment[18] confirmed that Ni films/colloids do not form in this reductive and acidic environment (Figure S8, SI).

$Ni_6(PET)_{12}$ as a Water Reducing Catalyst (WRC). To demonstrate its photocatalytic water reducing properties, the nickel cluster was used in a molecular system along with $[Ir(F\text{-}mppy)_2(dtbbpy)](PF_6)$ as the PS. The molecular structures of the two complexes used for the photoreactions are depicted in Figure 5. TEA functioned as the sacrificial reductant. For initial experiments, the PS concentration in the reaction vials was kept at 0.3 mM while a 0.025 mM catalyst concentration was chosen. Controls included vials without PS, WRC, water, or TEA. Figure 6 shows the H_2 evolution traces and corresponding catalyst turnover numbers (TONs) for the

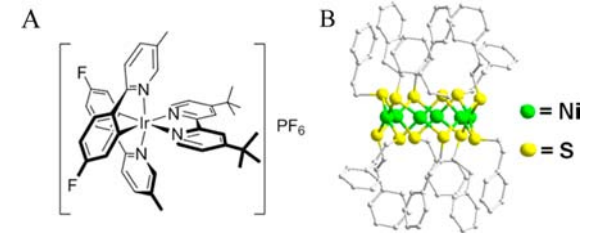

Figure 5. Molecular structures of (A) $[Ir(F\text{-}mppy)_2(dtbbpy)](PF_6)$ and (B) $Ni_6(PET)_{12}$.

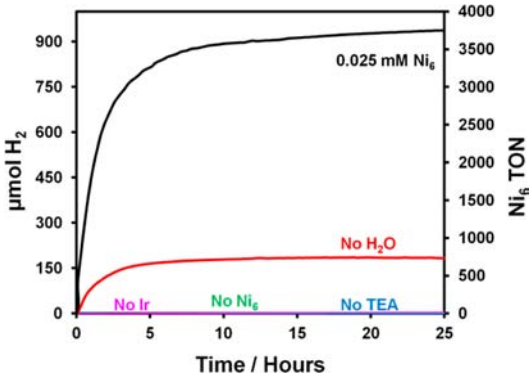

Figure 6. Performance evaluation of $Ni_6(PET)_{12}$ as WRC for photocatalytic H_2 generation (460 nm, 25 h) and comparison with controls. All reactions contained $[Ir(F\text{-}mppy)_2(dtbbpy)](PF_6)$ (0.3 mM) as the PS in a 10 mL 0.7 M solution of TEA in 90% THF−H_2O, unless otherwise stated.

systems. The vial containing all the components exhibited high catalyst turnovers (3750) while the controls evolved negligible H_2.

The vial without water, however, did produce up to 700 turnovers. This observation can be explained by the accepted reaction pathway which involves sequential electron transfers from the TEA and the resultant liberation of two protons.[19] It is important to note that 150 μmol H_2 could also be generated by a few milligrams of trace water present in the solvent. The rapid oxidation of TEA combined with the strong oxidizing nature of the excited state PS (E^*_{red} = +0.77 V) results in reductive quenching mechanism.[3b,20] To support this observation, a dynamic quenching study was performed using the Ir PS and the Ni cluster (experimental details given in the Supporting Information). A Stern−Volmer plot was generated (Figure 7) which gave a quenching constant, $k_q = 3.7 \times 10^9\ M^{-1}\ s^{-1}$ for the Ir(III) PS/Ni catalyst couple. Although the k_q for the catalyst is higher than that reported for TEA ($6.7 \times 10^7\ M^{-1}\ s^{-1}$, up to 0.1 M in 80% THF−water), the concentration of TEA in the actual photoreactions is 1000 times higher than the Ni_6 catalyst, implying that reductive quenching still prevails (Scheme 1). As demonstrated by the electrochemical HER study, Ni^{II} first undergoes a one electron reduction (via electron transfer from

dx.doi.org/10.1021/ic4013069 | Inorg. Chem. 2013, 52, 9094−9101

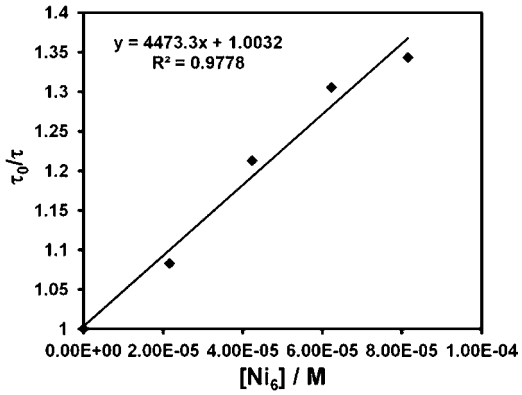

Figure 7. Stern–Volmer plot for $Ni_6(PET)_{12}$ as quencher. 0.02 mM $Ir(F\text{-}mppy)_2(dtbbpy)](PF_6)$ was used as the PS.

Scheme 1. H_2 Evolution by Reductive Quenching Mechanism

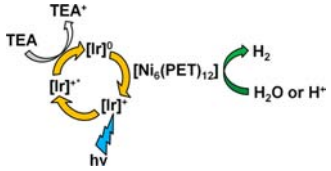

the reduced photosensitizer, $[Ir]^0$) and protonation, possibly yielding the formation of a hydride intermediate.[21] Subsequent reduction of an incoming proton would result in H_2 evolution.

To probe the mechanism further, concentrations of both, the PS and the WRC, were varied. Details of the effect of reactant concentration on H_2 evolution are depicted in Figure 8. In terms of catalyst turnovers, it was observed that the photocatalytic system performs best at high PS concentration and low WRC concentration (Figure 8A), while for PS turnovers, the trend is reversed (Figure 8B). These results point toward higher order degradation process of the WRC, like self-annihilation, which would be more prominent at higher concentrations. At the end of the photoreactions, the vials were also found to contain brown-black particulate matter, the amount increasing with catalyst concentrations. These observations again point toward catalyst degradation, evidence for which will be discussed below.

In order to explore the limit of this H_2 production system, the concentration of the catalyst was lowered from 0.025 mM to 0.0001 mM, keeping the PS at the optimal concentration (0.3 mM). Although there is an initial steady decrease in the quantity of hydrogen produced (Figure 9), hydrogen

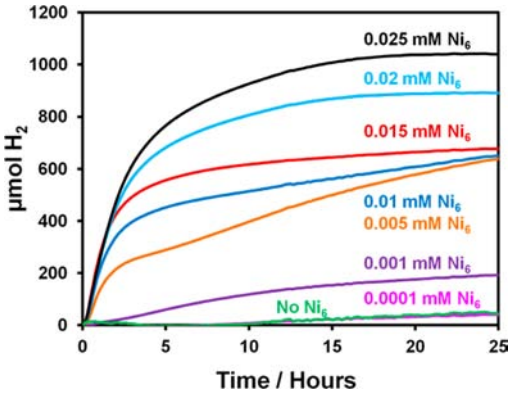

Figure 9. Kinetic traces at low $Ni_6(PET)_{12}$ concentrations with constant PS concentration of 0.3 mM in a 10 mL 0.7 M solution of TEA in 90% TH $-H_2O$. Decrease in higher order catalyst degradation leads to prolonged H_2 production, as shown by the traces for Ni concentrations lower than 0.015 mM (complete traces in SI).

production continued even after 90 h at lesser WRC concentrations (<0.015 mM, Figure S9, SI). This led to a substantial increase in turnovers, with 0.001 mM catalyst yielding up to 30 000 TON after 90 h. Time dependent spectroscopic analyses of select photoreaction mixtures (Figure S10, SI) show the gradual disappearance of Ni_6 absorption peaks and the presence of a new intense absorption at ~300 nm after 25 h of reaction time. This new feature could be tentatively assigned to Ni nanoparticles/colloids[22] or even smaller clusters/complexes, showing that the cluster disintegrates and corroborates the visual observation of particulate matter. Since the Ni_6 absorption features are retained during the first few hours of reaction (Figure S10 A,B, insets), it is proposed that the cluster itself is the active form, with the in-situ formed Ni particulate matter having little or no role to play in H_2 generation for higher catalyst concentrations. Even for the vials with low catalyst concentrations that produce H_2 even after 25 h, maximum activity is achieved during the first few hours as is evident from the traces depicted in Figure 9. Moreover, no new species can be detected spectroscopically during this time period (Figure S10 C). The slow, prolonged H_2 production could be due to a decrease in second-order catalytic degradation processes at low catalyst concentration. A similar trend was observed for Co-based catalysts at much

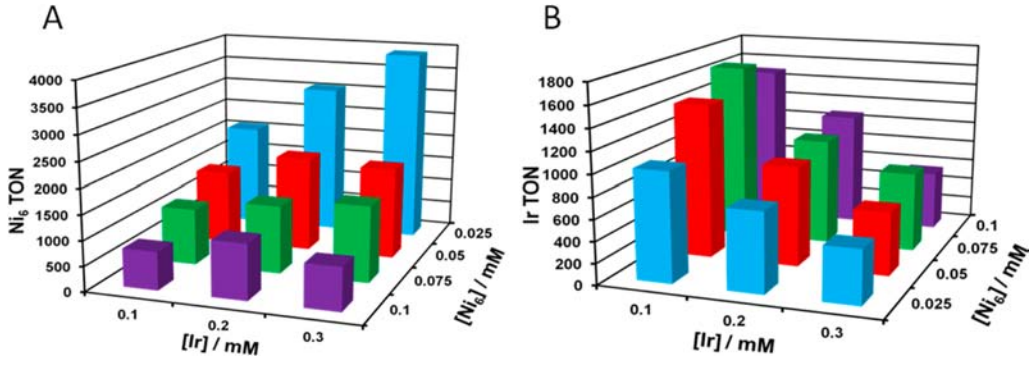

Figure 8. (A) Catalyst and (B) PS turnovers at varying concentrations of $Ir(F\text{-}mppy)_2(dtbbpy)](PF_6)$ and $Ni_6(PET)_{12}$ in a 10 mL 0.7 M solution of TEA in 90% THF–H_2O.

dx.doi.org/10.1021/ic4013069 | Inorg. Chem. 2013, 52, 9094–9101

lower H_2 yields.[23] Although nanostructured Ni-based catalysts have been used previously for H_2 generation,[22b,24] the activity of such catalysts is strongly affected by various factors like size, structure, particle dispersion, etc.[22c,25] In the present case, even if nanoparticles were formed in-situ, there would be a chance of aggregation/coalescence in the absence of stabilizing agents, making contributions from such components less likely. The reaction vial containing the least amount of catalyst (0.0001 mM) produced negligible H_2, similar to the control having no catalyst. Figure 10 shows the final catalyst turnovers for the entire concentration range used at 0.3 mM PS.

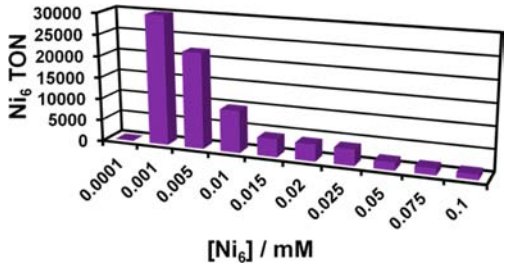

Figure 10. Final catalyst turnovers obtained at various concentrations of WRC in a 10 mL 0.7 M solution of TEA in 90% THF–H_2O (0.3 mM PS, 460 nm).

Comparison of the maximum catalyst turnover frequencies (TOFs) at different concentrations of WRC (Figure 11A) reveals that the reaction proceeds fastest at an optimal concentration (0.3 mM Ir and 0.025 mM Ni_6) achieving a maximum TOF of close to 1000 h^{-1}. The observed drop of TOFs at higher catalyst concentrations is consistent with the higher order degradation pathway suggested earlier. To determine the limit of the PS in the reactions, an additional experiment was carried out at higher PS concentrations. As seen previously, the water reduction system performs best at WRC concentrations of 0.025 mM, achieving up to 4700 turnovers (Figure S11, SI), further confirming the optimal concentration of the catalyst. Interestingly, no continuous increase in rate is detected on further increase of the PS concentration (Figure S12, SI). In fact, increasing the PS concentration from 0.3 mM to 1 mM decreases the rate by a factor of 4, denoting PS decay at higher concentrations. The corresponding results are depicted in Figure 11B.

Role of Particulate Matter in Photoreactions. To further ascertain the nature and role of the particulate matter formed during the photoreactions, a mercury poisoning experiment was performed by adding increasing equivalents of mercury to reaction vials containing 0.3 mM Ir and 0.1 mM Ni_6 catalyst. The reaction was carried out under vigorous stirring to facilitate proper mixing of the components. The corresponding H_2 evolution traces are depicted in Figure 12. It

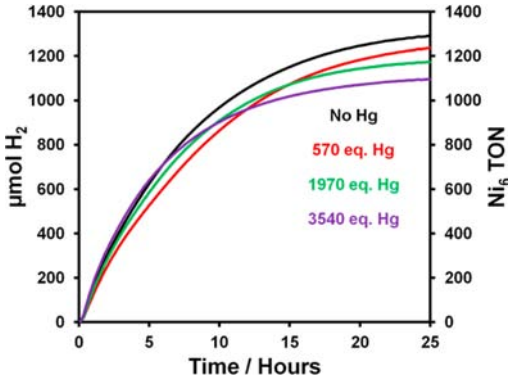

Figure 12. H_2 evolution traces for reaction vials containing 0.3 mM PS and 0.1 mM Ni_6, in presence of increasing equivalents of mercury.

can be seen that most of the catalytic activity is retained, even in the presence of over 3500 equivalents of Hg. This agrees with the evidence obtained in the photoreaction spectroscopic analyses that the species formed during photolysis do not take part in the generation of H_2. The small decrease in activity could be attributed to the increased obstruction of the light path with larger quantities of Hg. Previous studies done with Pd,[3c] for example, have shown a dramatic decrease in activity, something not seen in the present case. Remarkably, no loss of Hg properties (surface tension, luster, etc), commonly seen during amalgam formation was observed, hinting toward the non-metallic nature of the particulate matter.

It is evident that the processes governing these reactions are very complex. The H_2 evolution rate of the WRC cannot be considered as an isolated quantity, but it has to be placed in the context of the involved light absorption processes, electron transfer rates, degradation mechanism, etc. Making use of a versatile and robust Ir(III) PS and a Ni_6 thiolate WRC

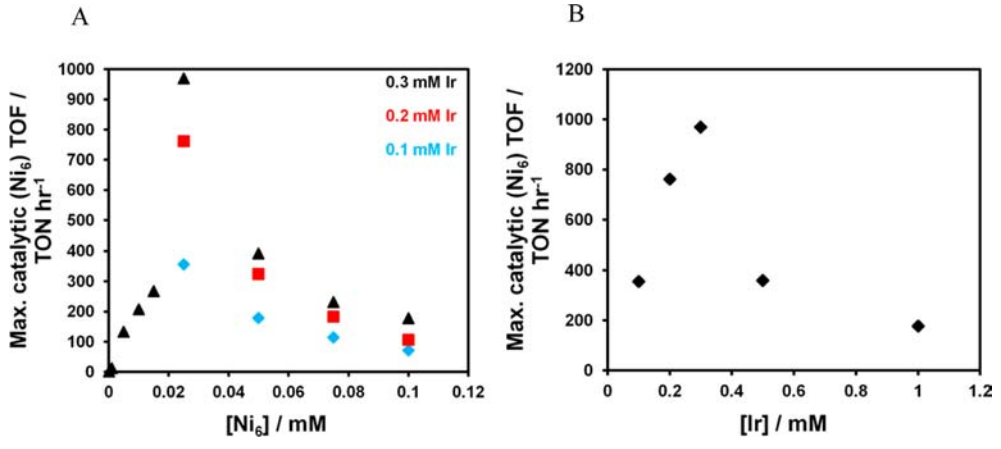

Figure 11. (A) Comparison of maximum catalyst turnover frequencies (TOFs) obtained at different PS and catalyst concentrations. (B) Effect of PS concentration on max. TOF, [Ni_6] = 0.025 mM.

dx.doi.org/10.1021/ic4013069 | Inorg. Chem. 2013, 52, 9094–9101

integrates all these factors, leading to a highly active water reduction system. It is an advantage that the Ni_6 cluster operates efficiently at low concentrations, even though the system is limited by catalytic degradation processes. It is possible that the active Ni_6 cluster disintegrates into smaller clusters or complexes during the course of photolysis. These new species are less likely to take part in the reactions, as was confirmed by UV−vis and mercury amalgam tests, indicating that this is a homogeneous water reduction system.

CONCLUSIONS

In summary, we report the use of an earth-abundant metal thiolate cluster, $Ni_6(SCH_2CH_2Ph)_{12}$, as a water reducing catalyst. Structure, purity, and stability of the Ni_6 complex were determined by several techniques, namely single crystal X-ray analysis, ^1H and 2D COSY NMR, ESI-MS, UV−vis spectroscopy, and TGA. Electrochemical analysis demonstrated HER activity of the catalyst in presence of a proton source (AcOH), via direct protonation of the reduced Ni(I) center. The water reduction property of the hexameric catalyst was evaluated using $[Ir(F\text{-}mppy)_2(dtbbpy)](PF_6)$ as PS with TEA as the sacrificial reductant. The system was found to perform optimally at 0.3 mM PS and 0.025 mM WRC concentrations, achieving maximum turnover numbers and turnover frequencies of 3750 and 970 TON h^{-1}, respectively. Close to 30 000 turnovers were obtained at low catalyst concentration of 0.001 mM and high PS concentrations, documenting the excellent performance of these clusters as WRCs. Dynamic quenching study of the Ir/Ni_6 couple and mercury poisoning tests revealed that the water reduction system proceeds through reductive quenching mechanism in a homogeneous manner.

ASSOCIATED CONTENT

Supporting Information

Experimental methods, crystallographic data of $Ni_6(PET)_{12}$, ESI-MS data, UV−vis studies, ^1H NMR stability study, cyclic voltammetry results, and additional photoreaction results. This material is available free of charge via the Internet at http://pubs.acs.org.

AUTHOR INFORMATION

Corresponding Author

*E-mail: bern@andrew.cmu.edu.

Author Contributions

The manuscript was written through contributions of all authors. All authors have given approval to the final version of the manuscript.

Notes

The authors declare no competing financial interest.

ACKNOWLEDGMENTS

The authors thank Anindita Das and James Woods for their assistance in the work. S.B. gratefully acknowledges support by the National Science Foundation (CHE-1055547). NMR instrumentation at CMU was partially supported by NSF (CHE-0130903 and CHE-1039870). R.J. acknowledges support by the AFOSR Award FA9550-11-1-9999 (FA9550-11-1-0147).

REFERENCES

(1) (a) Lewis, N. S.; Nocera, D. G. *Proc. Natl. Acad. Sci. U.S.A.* **2006**, *103*, 15729−15735. (b) McDaniel, N. D.; Bernhard, S. *Dalton Trans.* **2010**, *39*, 10021−10030.
(2) Du, P.; Eisenberg, R. *Energy Environ. Sci.* **2012**, *5*, 6012−6021.
(3) (a) Du, P.; Schneider, J.; Jarosz, P.; Zhang, J.; Brennessel, W. W.; Eisenberg, R. *J. Phys. Chem. B* **2007**, *111*, 6887−6894. (b) Cline, E. D.; Adamson, S. E.; Bernhard, S. *Inorg. Chem.* **2008**, *47*, 10378−10388. (c) Curtin, P. N.; Tinker, L. L.; Burgess, C. M.; Cline, E. D.; Bernhard, S. *Inorg. Chem.* **2009**, *48*, 10498−10506.
(4) (a) Probst, B.; Kolano, C.; Hamm, P.; Alberto, R. *Inorg. Chem.* **2009**, *48*, 1836−1843. (b) Probst, B.; Rodenberg, A.; Guttentag, M.; Hamm, P.; Alberto, R. *Inorg. Chem.* **2010**, *49*, 6453−6460. (c) McNamara, W. R.; Han, Z.; Alperin, P. J.; Brennessel, W. W.; Holland, P. L.; Eisenberg, R. *J. Am. Chem. Soc.* **2011**, *133*, 15368−15371.
(5) (a) McCormick, T. M.; Calitree, B. D.; Orchard, A.; Kraut, N. D.; Bright, F. V.; Detty, M. R.; Eisenberg, R. *J. Am. Chem. Soc.* **2010**, *132*, 15480−15483. (b) McLaughlin, M. P.; McCormick, T. M.; Eisenberg, R.; Holland, P. L. *Chem. Commun.* **2011**, *47*, 7989−7991.
(6) Carroll, M. E.; Barton, B. E.; Gray, D. L.; Mack, A. E.; Rauchfuss, T. B. *Inorg. Chem.* **2011**, *50*, 9554−9563.
(7) (a) Han, Z.; McNamara, W. R.; Eum, M. S.; Holland, P. L.; Eisenberg, R. *Angew. Chem., Int. Ed.* **2012**, *51*, 1667−1670. (b) Han, J.; Zhang, W.; Zhou, T.; Wang, X.; Xu, R. *RSC Adv.* **2012**, *2*, 8293−8296.
(8) (a) Woodward, P.; Dahl, L. F.; Abel, E. W.; Crosse, B. C. *J. Am. Chem. Soc.* **1965**, *87*, 5251−5253. (b) Dance, I. G.; Scudder, M. L.; Secomb, R. *Inorg. Chem.* **1985**, *24*, 1201−1208. (c) Angamuthu, R.; Kooijman, H.; Lutz, M.; Spek, A. L.; Bouwman, E. *Dalton Trans.* **2007**, *41*, 4641−4643. (d) Ivanov, S. A.; Kozee, M. A.; Merrill, W. A.; Agarwal, S.; Dahl, L. F. *J. Chem. Soc., Dalton Trans.* **2002**, *22*, 4105−4115. (e) Jian, F. F.; Jiao, K.; Li, Y.; Zhao, P. S.; Lu, L. D. *Angew. Chem., Int. Ed.* **2003**, *42*, 5722−5724. (f) Mahmoudkhani, A. H.; Langer, V. *Polyhedron* **1999**, *18*, 3407−3410. (g) Tan, C.; Jin, M.; Ma, X.; Zhu, Q.; Huang, Y.; Wang, Y.; Hu, S.; Sheng, T.; Wu, X. *Dalton Trans.* **2012**, *41*, 8472−8476. (h) Xiao, H. L.; Jian, F. F.; Zhang, K. J. *Bull. Korean Chem. Soc.* **2009**, *30*, 846−848. (i) Zhang, C.; Matsumoto, T.; Samoc, M.; Petrie, S.; Meng, S.; Christopher Corkery, T.; Stranger, R.; Zhang, J.; Humphrey, M. G.; Tatsumi, K. *Angew. Chem.* **2010**, *122*, 4305−4308.
(9) Angamuthu, R.; Bouwman, E. *Phys. Chem. Chem. Phys.* **2009**, *11*, 5578−5583.
(10) Zhang, W.; Hong, J.; Zheng, J.; Huang, Z.; Zhou, J.; Xu, R. *J. Am. Chem. Soc.* **2011**, *133*, 20680−20683.
(11) Lowry, M. S.; Hudson, W. R.; Pascal, R. A., Jr.; Bernhard, S. *J. Am. Chem. Soc.* **2004**, *126*, 14129−14135.
(12) (a) Brust, M.; Walker, M.; Bethell, D.; Schiffrin, D. J.; Whyman, R. *J. Chem. Soc., Chem. Commun.* **1994**, 801−802. (b) Zamborini, F. P.; Gross, S. M.; Murray, R. W. *Langmuir* **2001**, *17*, 481−488. (c) Qian, H.; Barry, E.; Zhu, Y.; Jin, R. *Acta Phys. Chim. Sin.* **2011**, *27*, 513−519. (c) Gottlieb, E.; Qian, H.; Jin, R. *Chem.—Eur. J.* **2013**, *19*, 4238−4243.
(13) Connelly, N. G.; Geiger, W. E. *Chem. Rev.* **1996**, *96*, 877−910.
(14) Qian, H.; Jiang, D.-e.; Li, G.; Gayathri, C.; Das, A.; Gil, R. R.; Jin, R. *J. Am. Chem. Soc.* **2012**, *134*, 16159−16162.
(15) Yang, Z.; Smetana, A. B.; Sorensen, C. M.; Klabunde, K. J. *Inorg. Chem.* **2007**, *46*, 2427−2431.
(16) (a) Kilgore, U. J.; Stewart, M. P.; Helm, M. L.; Dougherty, W. G.; Kassel, W. S.; DuBois, M. R.; DuBois, D. L.; Bullock, R. M. *Inorg. Chem.* **2011**, *50*, 10908−10918. (b) Han, J.; Zhang, W.; Zhou, T.; Wang, X.; Xu, R. *RSC Adv.* **2012**, *2*, 8293−8296.
(17) (a) Luca, O. R.; Blakemore, J. D.; Konezny, S. J.; Praetorius, J. M.; Schmeier, T. J.; Hunsinger, G. B.; Batista, V. S.; Brudvig, G. W.; Hazari, N.; Crabtree, R. H. *Inorg. Chem.* **2012**, *51*, 8704−8709. (b) Le Goff, A.; Artero, V.; Jousselme, B.; Tran, P. D.; Guillet, N.; Métayé, R.; Fihri, A.; Palacin, S.; Fontecave, M. *Science* **2009**, *326*, 1384−1387.
(18) Artero, V.; Fontecave, M. *Chem. Soc. Rev.* **2013**, *42*, 2338−2356.

(19) (a) Cohen, S. G.; Parola, A.; Parsons, G. H., Jr. *Chem. Rev.* **1973**, *73*, 141−161. (b) DeLaive, P. J.; Foreman, T. K.; Giannotti, C.; Whitten, D. G. *J. Am. Chem. Soc.* **1980**, *102*, 5627−5631.
(20) Lowry, M. S.; Goldsmith, J. I.; Slinker, J. D.; Rohl, R.; Pascal, R. A., Jr.; Malliaras, G. G.; Bernhard, S. *Chem. Mater.* **2005**, *17*, 5712−5719.
(21) (a) Zhang, W.; Wang, Y.; Wang, Z.; Zhong, Z.; Xu, R. *Chem. Commun.* **2010**, *46*, 7631−7633. (b) Assuncao, N.; De Giz, M.; Tremiliosi−Filho, G.; Gonzalez, E. *J. Electrochem. Soc.* **1997**, *144*, 2794−2800.
(22) (a) AlanáCreighton, J. *J. Chem. Soc., Faraday Trans.* **1991**, *87*, 3881−3891. (b) Zhang, W.; Xu, R. *Int. J. Hydrogen Energy* **2012**, *37*, 17899−17909. (c) Li, D.; Komarneni, S. *J. Am. Ceram. Soc.* **2006**, *89*, 1510−1517. (d) Knecht, M. R.; Garcia-Martinez, J. C.; Crooks, R. M. *Chem. Mater.* **2006**, *18*, 5039−5044.
(23) Goldsmith, J. I.; Hudson, W. R.; Lowry, M. S.; Anderson, T. H.; Bernhard, S. *J. Am. Chem. Soc.* **2005**, *127*, 7502−7510.
(24) (a) Domen, K.; Kudo, A.; Onishi, T.; Kosugi, N.; Kuroda, H. *J. Phys. Chem.* **1986**, *90*, 292−295. (b) Maeda, K.; Domen, K. *J. Phys. Chem. Lett.* **2010**, *1*, 2655−2661. (c) Agegnehu, A. K.; Pan, C.-J.; Rick, J.; Lee, J.-F.; Su, W.-N.; Hwang, B.-J. *J. Mater. Chem.* **2012**, *22*, 13849−13854. (d) van de Krol, R.; Liang, Y.; Schoonman, J. *J. Mater. Chem.* **2008**, *18*, 2311−2320.
(25) (a) Duteil, A.; Schmid, G.; Meyer-Zaika, W. *J. Chem. Soc., Chem. Commun.* **1995**, *1*, 31−32. (b) Schmid, G. In *Clusters and Colloids*. Wiley-VCH: New York, 2008.